clusters, the shape of the low end of the mass distribution in globular clusters will become amenable to direct measurement.

We have also detected six events that could indicate a hitherto unknown population of planetary-mass objects in M22. Our time series shows six brightening events that are completely unresolved in time (Fig. 2). In each event, the star is brighter than its average by ~0.3–0.8 mag at one epoch, and returns to normal brightness at the next epoch. The observations of each field were taken in pairs, separated by about 6 minutes. In each case, the brightening is observed in both images, as required by the microlensing interpretation—microlensing of a bulge star cannot be shorter than about 2 hours because of the finite size of the source. We have carefully inspected the point-spread functions in each image, and have ruled out artefacts and imperfections in the data reduction process—such as cosmic-ray hits or bad pixels—as the cause of the brightening. The positions and the baseline magnitudes of all the microlensed sources are given in Table 1.

The interpretation of these events as microlensing is necessarily tentative, because we do not have the usual confirmation tools of the shape and achromaticity of the light curve. On the other hand, we know of no stellar variability that could explain our observations. We can rule out two possibilities: flare stars and cataclysmic variables. Flare stars are generally M dwarfs[29], which—depending on the distance—would be either too faint or too red for the observed magnitudes and colours of these stars. Cataclysmic variables are generally blue, whereas all our candidates are red. On the other hand, the luminosity and amplitude distributions of the candidates are precisely those expected from microlensing of bulge stars. Their number distribution follows the distribution of the bulge stars, suggesting that they are bulge sources, and their amplitude distribution is consistent with their being due to microlensing. The contribution of these six unresolved events to the total microlensing optical depth is small, and their combined microlensing optical depth is consistent with the expected optical depth.

If these events indeed represent gravitational microlensing, the statistical upper limit to their duration (at a 95% confidence level) is 0.8 days, corresponding to a mass of only ~0.25 times that of Jupiter. These objects must be either free-floating, or at least several astronomical units from any stellar-mass object, otherwise the effect of the stellar object on the light curve would be easily detectable. The total contribution of these free-floating planets (if real) to the cluster mass is uncertain, but taking into account the area and the sensitivity of our monitoring programme, we estimate that this is of the order of 10%. Future multi-band observations at high time resolution could unambiguously establish the nature of such events, and would determine if they are indeed caused by detached planetary-mass objects. □

Received 28 March; accepted 2 May 2001.

1. Paczyński, B. Gravitational microlensing in the Local Group. *Annu. Rev. Astron. Astrophys.* **34,** 419–459 (1996).
2. Schneider, P., Ehlers, J. & Falco, E. E. *Gravitational Lenses* (Springer, Berlin, 1993).
3. Paczyński, B. Gravitational Microlensing by the Globular Cluster Stars. *Acta Astronomica* **44,** 235–239 (1994).
4. Paresce, F., De Marchi, G. & Romaniello, M. Very low mass stars and white dwarfs in NGC 6397. *Astrophys. J.* **440,** 216–226 (1995).
5. Elson, R. A. W., Gilmore, G. F., Santiago, B. X. & Casertano, S. HST observations of the stellar population of the globular cluster Ω Cen. *Astron. J.* **110,** 682–692 (1995).
6. King, I., Anderson, J., Cool, A. M. & Piotto, G. The luminosity function of the globular cluster NGC 6397 near the limit of hydrogen burning. *Astrophys. J.* **492,** L37–L40 (1998).
7. De Marchi, G. & Paresce, F. Low mass stars in globular clusters II. The mass function of M15. *Astron. Astrophys.* **304,** 202–210 (1995).
8. Burrows, A., Hubbard, W. B., Saumon, D. & Lunine, J. I. An expanded set of brown dwarf and very low mass star models. *Astrophys. J.* **406,** 158–171 (1993).
9. Gilliland, R. L. *et al.* A lack of planets in 47 Tucanae from a Hubble Space Telescope search. *Astrophys. J.* **545,** L47–L51 (2000).
10. Marcy, G. W., Butler, R. P. Planets orbiting other suns. *Publ. Astron. Soc. Pacif.* **112,** 137–140 (2000).
11. Alcock, C. *et al.* The MACHO project: microlensing results from 5.7 years of Large Magellanic Cloud observations. *Astrophys. J.* **542,** 281–307 (2000).
12. Afonso, C. *et al.* Microlensing towards the Small Magellanic Cloud EROS 2 two-year analysis. *Astron. Astrophys.* **344,** L63–L66 (1999).
13. Udalski, A. *et al.* The optical gravitational lensing experiment. Catalog of microlensing events in the galactic bulge. *Acta Astron.* **50,** 1–65 (2000).
14. Yanagisawa, T. *et al.* Wide-field camera for gravitational microlensing survey: MOA-cam2. *Exp. Astron.* **10,** 519–535 (2000).
15. Sahu, K. C. Stars within the Large Magellanic Cloud as potential lenses for observed microlensing events. *Nature* **370,** 275–276 (1994).
16. Sahu, K. C. Microlensing events of the LMC are better explained by stars within the LMC than by MACHOs. *Publ. Astron. Soc. Pacif.* **106,** 942–948 (1994).
17. Sahu, K. C. & Sahu, M. S. Spectroscopy of MACHO 97-SMC-1: Self-lensing within the Small Magellanic Cloud. *Astrophys. J.* **508,** L147–L150 (1998).
18. Cudworth, K. M. & Hansen, R. B. Space velocities of 14 globular clusters. *Astron. J.* **105,** 168–172 (1983).
19. Peterson, R. C. & Cudworth, K. M. Proper motions and radial velocities in the globular cluster M22 and the cluster distance. *Astrophys. J.* **420,** 612–631 (1994).
20. Stetson, P. B. in *Stellar Photometry—Current Techniques and Future Developments* (eds Butler, C. J. & Elliot, I.) 291–303 (IAU Colloq. 136, Cambridge Univ. Press, Cambridge, 1993).
21. Dominik, M. Galactic microlensing with rotating binaries. *Astron. Astrophys.* **329,** 361–374 (1998).
22. Paczynski, B. P. Binary source parallactic effect in gravitational micro-lensing. Preprint astro-ph/9711007 at ⟨http://xxx.lanl.gov⟩ (1997).
23. Freeman, K. C., de Vaucouleurs, G., Wainscoat, R. J. & de Vaucouleurs, A. A spectroscopic determination of the velocity dispersion in the Galactic bulge. *Astrophys. J.* **325,** 563–565 (1988).
24. Bode, M. F. & Evans, A. E. *Classical Novae* 5 (Wiley & Sons, Chichester, 1989).
25. Warner, B. *Cataclysmic variable Stars* 148 (Cambridge Univ. Press, Cambridge, 1995).
26. Downes, R. *et al.* A catalog and atlas of cataclysmic variables—the living edition. *Publ. Astron. Soc. Pacif.* (in the press).
27. Della Valle, M. & Livio, M. Are microlensing events contaminated by dwarf nova eruptions? *Astrophys. J.* **457,** L77–L79 (1996).
28. Samus, N., Kravtsov, V., Pavlov, M., Alcaino, G. & Liller, W. A new photographic colour-magnitude study of M 22 = NGC 6656. *Astron. Astrophys. Suppl. Ser.* **109,** 487–499 (1995).
29. Pettersen, B. R. A review of stellar flares and their characteristics. *Sol. Phys.* **121,** 299–312 (1989).

Acknowledgements

N.P. is on assignment from the Space Science Department of ESA. We thank H. Duerbeck, J. Valenti, H. Bond, R. Downes and J. Pringle for discussions.

Correspondence and requests for materials should be addressed to K.C.S. (e-mail: ksahu@stsci.edu).

Sub-poissonian loading of single atoms in a microscopic dipole trap

Nicolas Schlosser, Georges Reymond, Igor Protsenko & Philippe Grangier

Laboratoire Charles Fabry de l'Institut d'Optique, UMR 8501 du CNRS, BP 147, F91403 Orsay Cedex, France

The ability to manipulate individual atoms, ions or photons allows controlled engineering of the quantum state of small sets of trapped particles; this is necessary to encode and process information at the quantum level. Recent achievements in this direction have used either trapped ions[1–3] or trapped photons in cavity quantum-electrodynamical systems[3,4]. A third possibility that has been studied theoretically[5,6] is to use trapped neutral atoms. Such schemes would benefit greatly from the ability to trap and address individual atoms with high spatial resolution. Here we demonstrate a method for loading and detecting individual atoms in an optical dipole trap of submicrometre size. Because of the extremely small trapping volume, only one atom can be loaded at a time, so that the statistics of the number of atoms in the trap, N, are strongly sub-poissonian ($\Delta N^2 \approx 0.5N$). We present a simple model for describing the observed behaviour, and we discuss the possibilities for trapping and addressing several atoms in separate traps, for applications in quantum information processing.

Our experiment is based on the well developed methods of neutral-atom trapping and cooling. These techniques have already been used to prepare large samples of atoms in specific motional quantum states[7]. Individual atoms have been stored for short times in high-finesse optical cavities[8,9], and for longer times in weakly confining optical traps[10–12]. As far as quantum information

© 2001 Macmillan Magazines Ltd

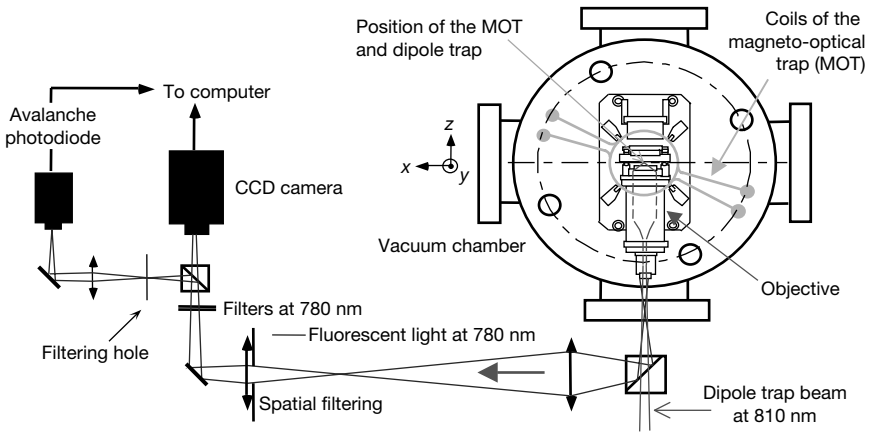

Figure 1 Main features of the experimental set-up. For simplicity, the slowing and MOT beams are not represented. A crucial feature of the experiment is the diffraction-limited (numerical aperture 0.7) focusing objective inside the vacuum chamber, which achieves submicrometre resolution. CCD, charge-coupled device.

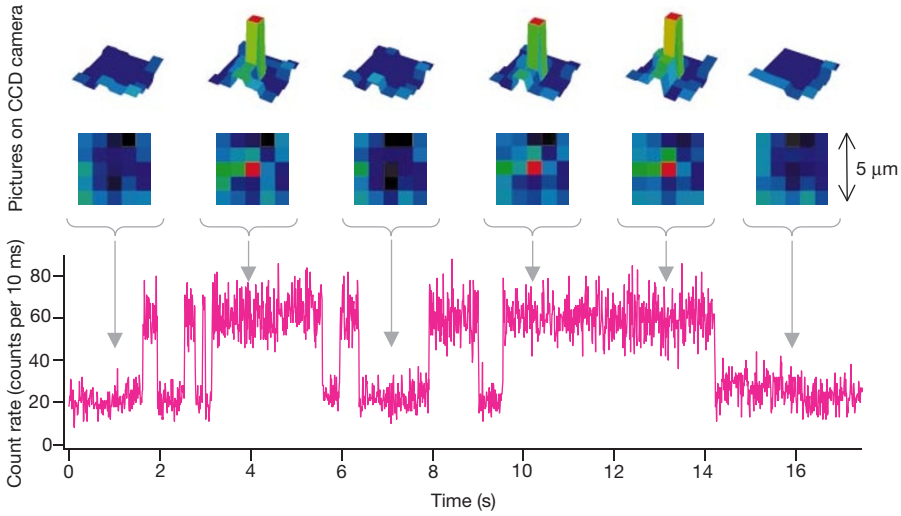

Figure 2 Single atom detection. Bottom, number of photons counted by an avalanche photodiode within 10-ms time bins. The steps correspond to either zero or one atom in the trap. Top, images of the trapped atom using a CCD camera. Squares (five pixels in side) around the trap image are shown, in a two- and three-dimensional view of selected images. The counting time for each image is 200 ms. The appearance of one trapped atom can be seen in real time.

processing with atomic qubits is concerned, controlled cold collisions[13] or atomic dipole–dipole coupling[14] have been proposed as new mechanisms for pairwise entanglement of neutral atoms. Such schemes can in principle be implemented in optical lattices with controlled filling[15], but loading and addressing individual trapping sites remains highly desirable[5,6]. In order to demonstrate the trapping and detection of a single ^{87}Rb atom with submicrometre resolution, we use a red-detuned optical dipole trap, which attracts the atoms towards regions of high field intensity, corresponding to the focus of the beam. A specific feature of our trap—which has not, to our knowledge, been achieved before—is an extremely small focal spot, which has a beam waist radius of $w_0 < 1\,\mu$m (see Methods section). It is thus possible to reach very high intensities ($100\,\mathrm{kW\,cm^{-2}}$) with a moderate input power (3 mW), and to confine the atom within a very small volume.

When both the dipole trap and the pre-cooling magneto-optical trap (MOT, see Fig. 1 and Methods section) are turned on together, a bright spot appears on a single pixel of the imaging CCD (charge-coupled device) camera (Fig. 2). A more detailed fit to the data shows that the fluorescent spot has a full-width at half-maximum of 0.7 μm in the object plane, which is the diffraction limit of the imaging system. For moderate loading of the trap and a dipole trap power of 1 mW, each atom scatters about 4,000 photons s^{-1} from the MOT beams. A blinking spot due to individual atoms entering and leaving the trap can thus easily be seen on the camera, using a counting time of 200 ms. The spot from the dipole trap is also imaged onto an avalanche photodiode (APD), which continuously counts photons within adjacent time bins. The detected fluorescence signal then exhibits characteristic steps, corresponding to individual atoms entering and leaving the trap. This behaviour is shown in Fig. 2, together with the CCD images, which are registered simultaneously.

A specific feature of our data, when compared to similar experiments using larger traps[12], is that count rates corresponding to more than one atom never occur. This statement can be made quantitative by using the histogram of counts shown in Fig. 3. The experimental data are compared with the histogram that can be expected from a compound Poisson law, which is fitted onto the peaks for $N = 0$ and $N = 1$. From these curves it is clear that the number of atoms N is strongly sub-poissonian (because $N = 2$ is missing), while the number of photons is approximately poissonian. The slight excess noise in the light (relative intensity of noise <10%) can be attributed mostly to technical noise in the MOT lasers.

The key feature of our data is the sub-poissonian character of the atom number[16,17]. By integrating the two fluorescence peaks shown in Fig. 3, we find that the probabilities of trapping N atoms

© 2001 Macmillan Magazines Ltd

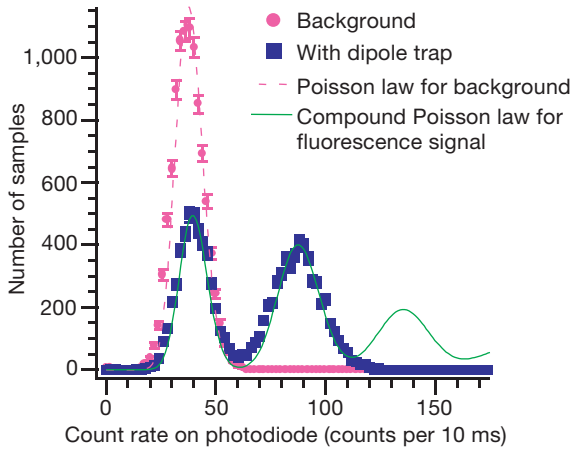

Figure 3 Sub-poissonian loading. The histogram of single-atom photon-counting data (Fig. 2) is displayed together with a compound Poisson law fitted to the 0-atom and 1-atom peaks. The 2-atom peak is clearly missing. The stray light background without the dipole trap is shown for comparison. Both histograms correspond to a total of 10,000 counting samples.

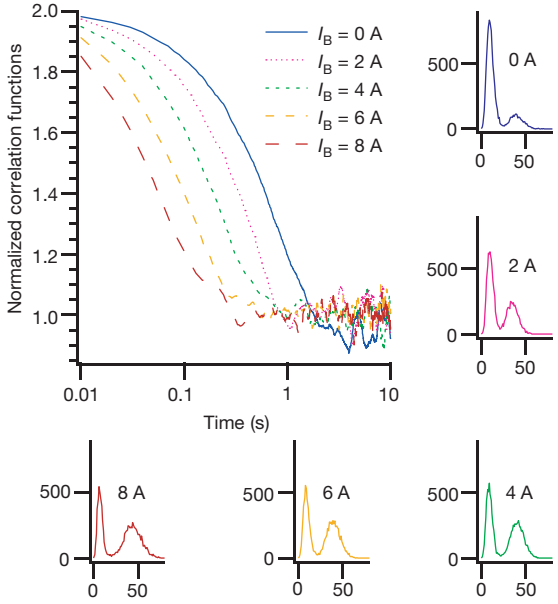

Figure 4 Intensity autocorrelations $g(t)$ of the MOT light emitted by the trapped atom (normalized for $g(0) = 2$ and $g(\infty) = 1$). The time behaviour is displayed together with selected histograms similar to the one shown in Fig. 3 (same axis labelling). The various curves are taken by increasing the MOT magnetic field B and thus the dipole trap loading rate. The current I_B for each magnetic field is given in amperes. The decreased storage time due to collisions leads to a faster swapping between zero and one atom. The histograms show again that there is never more than one atom in the trap.

are $p(N=0) \approx p(N=1) \approx 0.5$, and $p(N \geq 2) \approx 0$. This corresponds to $\Delta N^2 \approx 0.5N$, instead of the $\Delta N^2 = N$ that is expected for a Poisson law. Most of the observed features are very well reproduced by assuming that atoms enter the trap at random times, but that if an atom is already in the trap, both atoms escape. This model predicts that the '0 atom' and '1 atom' events have equal weights of 50%. The mechanism responsible for the escape can reasonably be attributed to collisions assisted by the MOT light, which have been shown to be crucial in larger dipole traps[18–20]. In practice, there might also be a collision with fast background atoms—this creates a trap lifetime which is typically a few seconds in our vacuum conditions.

A simple model combining this trap decay and the previously mentioned destructive two-body decay predicts a faster and faster swapping between no atoms and one atom in the trap when the loading rate is increased. We have checked this behaviour by measuring the autocorrelation of the detected fluorescence signal as a function of the loading rate (Fig. 4), and the observed results confirm that the correlation time is decreasing with increasing loading rate. In Fig. 4 we also show histograms—similar to those in Fig. 3—for various values of the magnetic field that controls the atomic density in the MOT (see Methods section). This confirms the following behaviour: for small loading rates, the lifetime of the trapped atom is equal to a constant value τ, essentially limited by collisions with fast atoms or molecules of the background gas, and the histograms show a majority of zero-atom periods, with long (several seconds) single-atom fluorescence periods. When the loading rate increases and becomes comparable to or larger than $1/\tau$, the probability of '1 atom' events increases, and quickly reaches its limit value of 50%. In this regime, the lifetime of the dipole trap decreases as the loading rate increases, following the statistics of the arrival of new atoms in the trap capture area.

For long-term storage of a single atom, the MOT is turned off 10 ms after an atom enters the trap, thereby stopping the loading and cooling processes, and only keeping the atom in the dipole trap. By turning on the MOT again after a given time, and measuring the probability that the atom is still in the dipole trap, the lifetime of the stored atom has been measured to be 2 s under typical experimental conditions.

Our set-up opens possibilities of exploring the proposed schemes for atom–atom entanglement. By simply sending another trapping beam at a small angle, and using the same optics, we have trapped two atoms at a controlled distance in the range 1–10 μm. After turning off the MOT beams, qubits can be implemented by using hyperfine sublevels of the atomic ground state[5,6,12]. Decoherence time, induced mostly by residual spontaneous emission from the dipole trap, and by intensity fluctuations of the trapping lasers, should be in the range 10–100 ms. One-qubit operations could be achieved by inducing Raman transitions between the hyperfine sublevels, separated by $\Delta\nu_H = 6.83$ GHz. Fast (microsecond) operation could be achieved by using as Raman beams the trapping laser itself, together with a pulsed control beam; the control beam would address each atom, and be detuned from the trapping beam by $\Delta\nu_H$.

For two-qubit operations, it should be possible to selectively couple one of the hyperfine sublevels to a high-n Rydberg state, by using a direct two-photon transition involving a pulsed blue laser and the trapping beam. Quite large two-photon effective Rabi frequencies would be easily accessible, owing to the very large intensity of the dipole trap beams. We have calculated that for two atoms separated by 3 μm, the dipole–dipole interaction between Rydberg states creates a level shift larger than 10 MHz. Moreover, a two-photon Rabi frequency of 200 kHz between the ground and Rydberg state should be accessible. Our set-up thus fulfils the basic requirements for realizing a fast C-NOT gate[21], with a switching time in the microsecond range. In principle, a three-atom scheme (Toffoli gate) could also be implemented along the same lines. □

Methods

Magneto-optical trap

The magneto-optical trap (MOT) uses a standard retroreflected 6 beam σ_+/σ_- configuration, except that the two beams within the plane of the coils (see Fig. 1) make a small angle of 20° (instead of the usual 90°), in order to fit within the optics of the focusing objective. The MOT is loaded from an atomic beam, slowed down by the usual chirped cooling method. Typically the MOT confines 10^7 atoms in a 1-mm-diameter cloud, with a density of about 10^{10} atoms cm^{-3}, or 0.01 atoms μm^{-3}. When correctly adjusted, the experiment can actually work without the slowing beams: the very small number of atoms that are captured by the MOT directly from the thermal atomic beam are enough to load the dipole trap. The loading rate is then approximately proportional to the MOT magnetic field; this is used for the experiment shown in Fig. 4.

© 2001 Macmillan Magazines Ltd

Optics

The focusing optics consists of two parts, which first focus and then re-collimate the beam for diagnostic purposes (see Fig. 1). Both parts have a numerical aperture of 0.7, a working distance of 1 cm, and a common focal point set at the centre of the MOT. The focusing objective consists of nine lenses, and achieves a diffraction-limited resolution of 0.7 μm, while the re-collimating objective consists of four lenses. The fluorescence light induced by the MOT beams is collected by the focusing objective, and gives a magnified image of the trap on a CCD camera. As the CCD camera has a slow response time, an APD is used in parallel, and monitors only the light coming from the trap region. Typically, the 1-μm-diameter dipole trap is imaged onto a 50-μm pinhole with a magnification of 20. The pulses from the APD are continuously registered by a computer, and can be processed to get histograms, intensity correlations, or photon counting statistics within the counting window.

Dipole trap

The linearly polarized dipole trap beam from a frequency stabilized titanium–sapphire laser is brought to the set-up using an optical fibre. Its wavelength is 810 nm, to be compared with the 795 nm (D1) and 780 nm (D2) lines of rubidium, so the trap operates far off resonance[22], where the spontaneous emission is very small. The typical oscillation frequency in the trap along the x–y (transverse) axes is calculated to be close to 200 kHz; this value has been confirmed experimentally by using parametric excitation of the oscillatory motion. The MOT cooling is expected to be working over a significant fraction of the potential well of the dipole trap. The trapped-atom temperature can be evaluated by measuring the fluorescence decay when turning off the MOT and dipole trap beams, and after some time turning on the MOT again. Data from the present experimental set-up, which is being improved, show that the trapped atom temperature is higher than 50 μK. An upper limit is given by the smallest potential for reliably trapping one atom, which is at present 1 mK. More accurate measurements of the temperature and motional properties of the trapped atom are under way.

Received 14 March; accepted 11 May 2001.

1. Sackett, C. A. *et al.* Experimental entanglement of four particles. *Nature* **404,** 256–259 (2000).
2. Steane, A. *et al.* Speed of ion-trap quantum-information processors. *Phys. Rev. A* **62,** 042305-1–042305-9 (2000).
3. Walther, H. Single atom experiments in cavities and trap. *Proc. R. Soc. Lond. A* **454,** 431–445 (1998).
4. Rauschenbeutel, A. *et al.* Coherent operation of a tunable quantum phase gate in cavity QED. *Phys. Rev. Lett.* **83,** 5166–5169 (1999).
5. Calarco, T., Briegel, H. J., Jaksch, D., Cirac, J. I. & Zoller, P. Entangling neutral atoms for quantum information processing. *J. Mod. Opt.* **47,** 2137–2149 (2000).
6. Brennen, G. K., Deutsch, I. H. & Jessen, P. S. Entangling dipole-dipole interactions for quantum logic with neutral atoms. *Phys. Rev. A* **61,** 062309-1–062309-10 (2000).
7. Morinaga, M., Bouchoule, I., Karam, J. C. & Salomon, C. Manipulation of motional quantum states of neutral atoms. *Phys. Rev. Lett.* **83,** 4037–4040 (1999).
8. Doherty, A. C., Lynn, T. W., Hood, C. J. & Kimble, H. J. Trapping of single atoms with single photons in cavity QED. *Phys. Rev. A* **63,** 013401-1–013401-24 (2001).
9. Pinkse, P. W. H., Fischer, T., Maunz, P. & Rempe, G. Trapping an atom with single photons. *Nature* **404,** 365–368 (2000).
10. Hu, Z. & Kimble, H. J. Observation of a single atom in a magneto-optical trap. *Opt. Lett.* **19,** 1888–1890 (1994).
11. Ruschewitz, F., Bettermann, D., Peng, J. L. & Ertmer, W. Statistical investigations on single trapped neutral atoms. *Europhys. Lett.* **34,** 651–656 (1996).
12. Frese, D. *et al.* Single atoms in an optical dipole trap: towards a deterministic source of cold atoms. *Phys. Rev. Lett.* **85,** 3777–3780 (2000).
13. Calarco, T. *et al.* Quantum gates with neutral atoms: Controlling collisional interactions in time-dependent traps. *Phys. Rev. A* **61,** 022304-1–022304-11 (2000).
14. Brennen, G. K., Caves, C. M., Jessen, P. S. & Deutsch, I. H. Quantum logic gates in optical lattices. *Phys. Rev. Lett.* **82,** 1060–1063 (1999).
15. DePue, M. T. *et al.* Unity occupation of sites in a 3D optical lattice. *Phys. Rev. Lett.* **82,** 2262–2265 (1999).
16. Rempe, G. & Walther, H. Sub-Poissonian atomic statistics in a micromaser. *Phys. Rev. A* **42,** 1650–1655 (1990).
17. Orzel, C., Tuchman, A. K., Fenselau, M. L., Yasuda, M. & Kasevich, M. A. Squeezed states in a Bose-Einstein condensate. *Science* **291,** 2386–2389 (2001).
18. Gensemer, S. D., Gould, P. L., Leo, P. J., Tiesinga, E. & Williams, C. J. Ultracold ^{87}Rb ground-state hyperfine-changing collisions in the presence and absence of laser light. *Phys. Rev. A* **62,** 030702-1–030702-4 (2000).
19. Nesnidal, R. C. & Walker, T. G. Light-induced ultracold spin-exchange collisions. *Phys. Rev. A* **62,** 030701-1–030701-4 (2000).
20. Kuppens, S. J. M., Corwin, K. L., Miller, K. W., Chupp, T. E. & Wieman, C. E. Loading an optical dipole trap. *Phys. Rev. A* **62,** 013406-1–013406-13 (2000).
21. Jaksch, D. *et al.* Fast quantum gates for neutral atoms. *Phys. Rev. Lett.* **85,** 2208–2211 (2000).
22. Miller, J. D., Cline, R. A. & Heinzen, D. J. Far-off-resonance optical trapping of atoms. *Phys. Rev. A* **47,** R4567– R4570 (1993).

Acknowledgements

The contributions of K. Vigneron, H. Wilhelm and T. Zhang to early stages of the experiment are acknowledged. This work was supported by the European IST/FET programme 'QUBITS' and by the European IHP network 'QUEST'.

Correspondence and requests for materials should be addressed to P.G. (e-mail: philippe.grangier@iota.u-psud.fr).

Nonlinear limits to the information capacity of optical fibre communications

Partha P. Mitra & Jason B. Stark

Bell Laboratories, Lucent Technologies, Murray Hill, New Jersey 07974, USA

The exponential growth in the rate at which information can be communicated through an optical fibre is a key element in the 'information revolution'. However, as for all exponential growth laws, physical limits must be considered. The nonlinear nature of the propagation of light in optical fibre has made these limits difficult to elucidate. Here we use a key simplification to investigate the theoretical limits to the information capacity of an optical fibre arising from these nonlinearities. The success of our approach lies in relating the nonlinear channel to a linear channel with multiplicative noise, for which we are able to obtain analytical results. In fundamental distinction to linear channels with additive noise, the capacity of a nonlinear channel does not grow indefinitely with increasing signal power, but has a maximal value. The ideas presented here may have broader implications for other nonlinear information channels, such as those involved in sensory transduction in neurobiology. These have been often examined using additive noise linear channel models[1] but, as we show here, nonlinearities can change the picture qualitatively.

The classical theory of communications[1] was developed mostly in the context of linear channels with additive noise, which was adequate for electromagnetic propagation through wires and cables that have until recently been the main conduits for information flow. Fading channels or channels with multiplicative noise have been considered, for example in the context of wireless communications[2], although such channels remain theoretically less tractable than the additive noise channels. However, with the advent of optical fibre communications we are faced with a nonlinear propagation channel that poses major challenges to our understanding. The difficulty is that the input–output relationship of an optical fibre channel is obtained by integrating a nonlinear partial differential equation and may not be represented by an instantaneous nonlinearity. Channels where the nonlinearities in the input–output relationship are not instantaneous are in general ill understood, the optical fibre simply being a case of current relevance. The understanding of such nonlinear channels with memory are of fundamental interest, both because communication rates through optical fibre are increasing exponentially and we need to know where the limits are, and also because understanding such channels may give us insight elsewhere, such as into the design principles of neurobiological information channels at the sensory periphery.

The capacity of a communication channel is the maximal rate at which information may be transferred through the channel without error. The capacity can be written as a product of two conceptually distinct quantities, the spectral bandwidth W and the maximal spectral efficiency which we will denote C'. In the classic capacity formula for the additive white gaussian noise channel with an average power constraint, $C = W \log_2(1 + S/N)$, the spectral bandwidth W, which has dimensions of inverse time, multiplies the dimensionless maximal spectral efficiency $C' = \log_2(1 + S/N)$ (sometimes written with 'units' of bits s^{-1} Hz^{-1}). Here S and N are the signal and noise powers respectively. As the maximal spectral efficiency is logarithmic in the signal to noise ratio (S/N), the capacity is principally determined by the bandwidth W. In the case of an optical fibre, the intrinsic loss mechanisms of light propagating

© 2001 Macmillan Magazines Ltd